Article

Discovery Medicine 2026; 38(204): 171–187
https://doi.org/10.24976/Discov.Med.202638204.14

Butyrate Enhances Anti-PD-1 Antitumor Efficacy in Lung Cancer via Modulating STAT1/IDO1-Mediated Tryptophan-Kynurenine Pathway

Chuanchuan Li[1], Xixi Li[2], Bo Ma[3], Feng Yuan[1], Shouzhong Wang[4], Weixian Liu[5,*]

[1]Department of Thoracic Surgery, Zhejiang Hospital, 310000 Hangzhou, Zhejiang, China
[2]Department of Orthopedics, Zhejiang Hospital, 310000 Hangzhou, Zhejiang, China
[3]Department of Breast Surgery, Zhejiang Hospital, 310000 Hangzhou, Zhejiang, China
[4]Department of Medical Oncology, Zaozhuang Chest Hospital, 277500 Zaozhuang, Shandong, China
[5]Department of Neurosurgery, Zhejiang Hospital, 310000 Hangzhou, Zhejiang, China
*Correspondence: 20214133110@stu.edu.suda.cn (Weixian Liu)
Submitted: 23 October 2025 Revised: 4 December 2025 Accepted: 16 December 2025 Published: 20 January 2026

Background: While programmed death 1 (PD-1) inhibitors have shown remarkable efficacy and survival benefits in lung cancer, their clinical utility is limited when used alone. This study aims to investigate the underlying mechanism by which sodium butyrate (NaB), combined with PD-1 inhibitors, enhances immunotherapeutic efficacy of lung cancer via modulating the signal transducer and activator of transcription 1 (STAT1)/Indoleamine 2, 3-dioxygenase 1 (IDO1)-activated tryptophan (Trp)-kynurenine (Kyn) pathway.

Methods: To assess the effect of combining NaB with a PD-1 inhibitor on lung cancer, we employed a comprehensive array of techniques, including live animal imaging, hematoxylin and eosin (H&E) staining, immunohistochemical analysis, enzyme-linked immunosorbent assay (ELISA), flow cytometry, and various biochemical tests.

Results: Our findings indicated that NaB had the potential to dramatically slow down tumor progression, promote cancer cell death, decrease the ratio of kynurenine to tryptophan, boost the efficacy of PD-1 inhibitors through impeding STAT1/IDO1 pathway ($p < 0.05$), thereby bolstering the body's anti-cancer response. Meanwhile, co-administration of NaB and PD-1 inhibitor activated $CD8^+$ T cells to trigger apoptosis, inhibited tumor cell proliferation, and reduced the Kyn content *in vitro* ($p < 0.05$). Moreover, NaB, coupled with a PD-1 inhibitor, down-regulated p-STAT1, IDO1, and programmed death-ligand 1 (PD-L1) protein expression in $CD8^+$ T cells and Lewis lung carcinoma (LLC) co-cultured system ($p < 0.05$). However, the occurrence of the above results was abolished by 2-(1, 8-Naphthyridin-2-yl)phenol (2-NP) or 6-Formylindolo[3, 2-b]carbazole (FICZ) ($p < 0.05$).

Conclusion: Collectively, our findings revealed that NaB ameliorates the immunosuppressive surroundings in lung cancer and enhances the effect of PD-1 inhibitor through STAT1/IDO1-mediated tryptophan and kynurenine metabolism.

Keywords: lung cancer; butyrate; programmed death 1; IDO1; tryptophan

Introduction

Lung cancer (LC) ranks as the primary oncological cause of mortality globally, accounting for an estimated 1.8 million deaths (18.7%) [1]. Non-Small Cell Lung Cancer (NSCLC) constitutes 85% of diagnoses, typically discovered at advanced stages that prohibit surgery [2]. Although platinum-based combination therapy remains the primary approach for advanced NSCLC [3], further improvements in patient survival have stagnated. Molecular targeted therapy has yielded remarkable outcomes, but there is still a lack of particularly effective treatment for patients with negative driver gene sensitive mutations or after drug resistance [4,5]. Cancer cells avoid immune recognition through surface programmed death-ligand 1 (PD-L1) expression, binding to T cell programmed death 1 (PD-1) receptors [6]. PD-1, a crucial immune checkpoint, is overexpressed on T cells in the tumor microenvironment, contributing to immune suppression. PD-1 and PD-L1 inhibitors have been authorized for treating NSCLC, but monotherapy effectiveness remains limited [7]. Moreover, their application is restricted because of their toxic side effects and poor tolerability [8]. Hence, exploring more effective treatment modalities for anti-lung cancer in clinics is urgent.

Emerging evidence shows that specific microbiota-derived metabolites contribute crucially to cancer prevention and supportive therapy [9]. Recent research indicates that the bacteria *Clostridium butyricum* can bolster the effectiveness of immune checkpoint inhibitors for treating renal cell carcinoma, thereby considerably extending the duration of remission in patients [10]. Butyrate, produced by *Clostridium butyricum*, confers health advantages, including immune modulation and tumor suppression. It achieves

immunomodulatory effects by regulating inflammatory factor expression through multiple signaling pathways [11]. It suppresses pro-inflammatory interleukin-1β (IL-1β) and IL-6 while enhancing anti-inflammatory IL-10 expression. Moreover, butyrate potentiates $CD8^+$ T cell antitumor immunity and modulates the function, proliferation, and programmed cell death of diverse immune cells [12,13]. Previous study has shown that NSCLC patients exhibit distinct gut microbiota compared to healthy adults and frequently encounter dysbiosis of the butyrate-producing bacteria within their intestinal tracts [14]. Furthermore, serum butyrate concentrations correlate with the efficacy of anti-PD-1 treatments in NCLC individuals [15]. However, its mechanisms remain unclear in lung cancer.

Butyrate modulates the anti-tumor $CD8^+$ T cell response by activating inhibitor of DNA binding 2 (ID2)-mediated IL-12 signaling [12]. Remarkably, butyrate suppresses Interferon-gamma (IFN-γ)-induced signal transducer and activator of transcription 1 (STAT1) phosphorylation, subsequently reducing Indoleamine 2, 3-dioxygenase 1 (IDO1) expression in human intestinal epithelial cells [16]. Metabolism of L-Tryptophan (Trp) through the kynurenine (Kyn) route influences immune responses, neural activity, and gut stability [17]. IDO1 is an essential endogenous inhibitor in the body, with elevated expression in tumor cells [18]. Activated $CD8^+$ T cells release IFN-γ within the tumor microenvironment, engaging tumor cell receptors to induce STAT1 phosphorylation. This activated STAT1 forms nuclear homodimers that upregulate IDO1 expression. Some preclinical trials have found that IDO1 inhibitors activate immunity and make effector T cells proliferate [19]. Concurrent use of immune checkpoint inhibitors (ICIs) enhances tumor suppression over monotherapy with ICIs. However, the fundamental mechanisms by which butyrate modulates IDO1 in lung cancer remains incompletely understood.

In the current study, this study aims to explore whether the combination of butyrate and PD-1 inhibitors may enhance immunotherapeutic efficacy of lung cancer by regulating the STAT/IDO1 axis. As a result, our research indicates that butyrate can improve the immunosuppressive microenvironment in lung cancer, thus enhancing the effectiveness of PD-1 inhibitors by regulating IDO1-driven tryptophan degradation, providing a new direction for developing novel therapeutics for preventing lung cancer.

Materials and Methods

Cell Culture

Mouse Lewis lung carcinoma (LLC) cells and LLC luciferase (LLC-Luc) cells were acquired from the Chinese Academy of Sciences Cell Bank (iCell-m027, iCell-0078a, Cellverse, Shanghai, China). Cell line authenticity was confirmed by STR profiling, validating their murine LLC cell characteristics without contamination. Besides, all cells tested negative for mycoplasma prior to use. Cells were maintained in Dulbecco's Modified Eagle Medium (DMEM) with 10% fetal bovine serum (FBS) (BS1105, Inner Mongolia Opsai Biotechnology, China), 100 µg/mL streptomycin (GNM15140-1, Zhejiang Jinuo Saibai'er Biotechnology Co., Ltd., Zhejiang, China) and 100 U/mL penicillin (A1170, Solarbio, Beijing, China) in a 5% CO_2 humidified environment at 37 °C.

Animal Study and Bioluminescence Imaging

Male C57BL/6 mice (18–22 g, aged 6–8 weeks) were obtained from SLAC (Shanghai, China) and housed in a specific pathogen-free (SPF) conditions at 22 $\pm$ 2 °C with 60%–80% humidity and had unrestricted access to food and water. A total of 30 mice were intravenously injected with 100 µL of LLC-luc cell suspension (1×10^7 cells/mL in phosphate-buffered saline (PBS)) via the tail veins [20,21], and additional 6 mice were selected as the control group receiving 0.1 mL PBS intravenously. The LC mice were segregated and randomly assigned to five groups after 7 days: the Model group, the Anti-PD-1 (865024J1C, Novo Nordisk, Tianjin, China) group, the Anti-PD-1+low dosage sodium butyrate (NaBL) (#303410, Sigma, MO, USA) group, the Anti-PD-1+midium dosage NaB (NaBM) group, the Anti-PD-1+high dosage NaB (NaBH) group (n = 6). Mice in the Anti-PD-1 group were administered 200 µg of anti-PD-1 antibody via intraperitoneal injection every other day. Mice in the NaB combination groups received daily intraperitoneal injections of NaB at doses of 100 mg/kg (NaBL), 200 mg/kg (NaBM), or 300 mg/kg (NaBH), in addition to 200 µg of anti-PD-1 antibody every other day. Mice in the Control and Model groups were injected intraperitoneally with an equal volume of sterile isotonic saline (0.4 mL) every day, and fed with normal drinking water. Following 4 weeks of consecutive treatment, bioluminescence of mice was detected through live imaging (AniView 100, Biolight Biotechnology Co., Ltd., Guangzhou, China) with 15 mg/mL D-luciferin (10 µL/g body weight, #ST196, Beyotime, China). Finally, mice were anesthetized with 3% isoflurane (R510-22-10, RWD, Shenzhen, China) using a Rodent Anesthesia Machine (ABS-4A1, Yuyan Instruments Co., Ltd., Shanghai, China) and euthanized by cervical dislocation. Then, the thymus and spleen tissues were excised and weighed to calculate the thymus index and spleen index according to the formula: Organ index = organ weight/body weight (mg/g). The animal experiments were approved by the Ethics Committee of Hangzhou Hunter Testing Biotechnology Co., Ltd. (NO. IACUC/HTYJ-8201-80), and all efforts were made to minimize suffering and ensure animal welfare throughout the study.

Quantification of Trp and Kyn by HPLC Analysis

Lung tumor samples were processed by homogenizing 1 mL of tissue in chilled methanol via ultrasonication. The

supernatant, obtained after centrifugation at 12,000 rpm for 10 min, was analyzed by HPLC (U3000, Thermo fisher, MA, USA). Separation was performed using an ExionLC AD UHPLC system equipped with an ACQUITY UPLC HSS T 3 column (4 µL injection volume), maintaining the column at 40 °C and the injection plate at 4 °C.

Enzyme-Linked Immunosorbent Assay (ELISA) Analysis

Following anesthesia, blood was collected from the enucleated eyeballs of mice in each group. The samples were then centrifuged at 3000 r/min for 20 min at 4 °C to isolate the serum. Then, the serum IL-2, tumor necrosis factor alpha (TNF-α), and IFN-γ levels were tested with commercial ELISA kits (RX203061M, RX202412M, RX203097M, Quanzhou Rui Xin Biotechnology Co., Ltd., China). Additionally, the levels of Kyn in the cell culture supernatants were measured by ELISA (CB11300, COIBO BIO, Shanghai, China) according to the manufacturer's instructions.

Hematoxylin and Eosin (H&E) Staining

Lung tumor tissues were fixed in 4% paraformaldehyde for 24 h, thoroughly dehydrated through a series of graded ethanol and xylene, and subsequently embedded in paraffin blocks. Tissue sections (4 µm) were prepared and subjected to a standard H&E staining protocol. Briefly, after deparaffinization and rehydration, sections were stained with hematoxylin (H3136, Sigma, MO, USA), differentiated, blued, and counterstained with eosin (E4009, Sigma, MO, USA). The stained sections were then dehydrated, cleared, and coverslipped for microscopic examination (Eclipse Ci-L, Nikon, Japan).

Terminal Deoxynucleotidyl Transferase (TdT) dUTP Nick-End Labeling (TUNEL) Staining

Apoptosis in paraffin-embedded lung cancer tissues was detected using the One-Step TUNEL Apoptosis Assay Kit (C1090, Beyotime). Briefly, tissue sections were deparaffinized in xylene and rehydrated through a graded ethanol series to distilled water. Sections underwent heat-mediated antigen retrieval in sodium citrate buffer (10 mM, pH 6.0) at 95 °C for 15 min and then were allowed to cool naturally to room temperature. After washing with PBS, the sections were permeabilized with 20 µg/mL Proteinase K (ST532, Beyotime) for 20 min at 37 °C and rinsed again. The TUNEL reaction mixture was prepared according to the manufacturer's instructions and added to the tissue sections, which were then incubated in a dark, humidified chamber at 37 °C for 60 min. Following incubation, the sections were washed thoroughly to terminate the reaction. After a final wash, the sections were mounted with an anti-fade mounting medium with DAPI (ab104139, Abcam). Apoptotic cells, identified by red TUNEL fluorescence, were visualized and quantified from five random fields per section using Image-Pro Plus software (version 6.0; Media Cybernetics, Rockville, MD, USA).

Immune Cells Infiltration Analysis

Peripheral blood mononuclear cells (PBMCs) of LC mice were isolated from the blood sample according to the instructions provided in the Mouse Peripheral Blood Lymphocyte Separation Kit (P8620, Solarbio, Beijing, China). Briefly, blood samples were layered over the separation medium. After centrifugation, the separated liquid layer was carefully aspirated and transferred to a new centrifuge tube. The cells were then washed 2–3 times with PBS by centrifugation and resuspended in PBS. Next, the lymphocyte suspensions were stained with 20 µL each of FITC anti-CD25 (abs182339, Absin, Shanghai, China) and APC anti-CD4 antibodies (sc-20079 PE, 1:20 dilution, SANTA CRUZ) and incubated in the dark for 20 min. Subsequently, the proportioned membrane-breaking agent was added, and PE anti-Foxp3 mAb (sc-53876 PerCP, 1:20, SANTA CRUZ) was added and incubated in the dark for another 20 min. Finally, the percentage of Foxp3-expressing CD4($^+$) regulatory T (Treg) cells in LC mice was measured using flow cytometry (NovoCyte, Agilent) and analyzed using FlowJo software (v10, BD Biosciences).

Immunohistochemistry (IHC) Analysis

Paraffin tumor sections were deparaffinized with 3% H_2O_2, blocked with 5% goat serum, then incubated with primary antibody anti-CD4 (bs-0766R, 1:200, BIOSS), anti-CD8α (ab217344, 1:2000, Abcam), anti-IDO1 (ab311847, 1:1000, Abcam), and anti-p-STAT1 (ab109461, 1:200, Abcam) overnight at 4 °C. Sections were stained with HRP-conjugated secondary antibody (ab97080, 1:500, Abcam) and observed under a Nikon DS-U3 microscope (Nikon DS-U3, Japan). The density of target proteins was measured by calculating average optical density (AOD) using ImageJ software (version 1.53; NIH, Bethesda, MD, USA).

Preparation of Mouse CD8$^+$ T Cells

The spleen tissue was taken and placed in precooled PBS and then ground on a filter with a grinding rod. Following centrifugation of the ground liquid, red blood cells were lysed and splenocytes were resuspended in MACS buffer, PBS supplemented with 0.5% BSA (ST023, Beyotime, Shanghai, China) and 2 mM EDTA (ST1303, Beyotime). Next, mouse CD8$^+$ T cells were purified by MACS using the CD8$^+$ T Cell Isolation Kit (130-090-859, Miltenyi Biotec Inc, Cologne, Germany) according to the manufacturer's instructions. CD8$^+$ T lymphocytes were identified by flow cytometry, and the proportion of CD3$^+$/CD8$^+$ cell subsets was measured . Briefly, 200 µL of splenocyte suspension (2×10^6 cells) was incubated with 1 µL of CD3-FITC (E-AB-F1013C, Elabscience, Wuhan, China) and 1 µL of CD8-PE (E-AB-F1104E, Elabscience) for 30 min in the dark. After incubation, the cells were resuspended in

500 µL of PBS and analyzed by flow cytometry. The percentage of $CD8^+$ T lymphocyte subset ($CD3^+/CD8^+$) was subsequently calculated. $CD8^+$ T cells were cultured in RPIM-1640 medium (Quanshijin Biotechnology Co., Ltd., Beijing, China) with 10% FBS and 2 mM glutamine (25-005-CI, Corning, USA) at 37 °C in 5% CO_2.

Cell Counting Kit-8 (CCK-8) Assay

Lung cancer and were co-cultured with mouse $CD8^+$ T cells, which were added at a density of 0.1 mL per well. The LLC cells were categorized into six groups: blank control group, $CD8^+$ T cells group, $CD8^+$ T cells co-culture + PD-1 inhibitor (25 mg/mL, camrelizumab) group, $CD8^+$ T cells co-culture + PD-1 inhibitor + butyrate (10 mmol/L) group, $CD8^+$ T cells co-culture + PD-1 inhibitor + butyrate + STAT1 agonist (2-(1, 8-Naphthyridin-2-yl)phenol, 2-NP, 10 mM, HY-W013523, MedChemExpress, New Jersey, USA) group, $CD8^+$ T cells co-culture + PD-1 inhibitor + butyrate + AhR receptor agonist (6-Formylindolo[3, 2-b]carbazole, FICZ, 10 µM, HY-12451, MedChemExpress) group. Following drug administration and supplementation with 0.7 mM exogenous tryptophan, cells underwent 48 h of co-culture. Following incubation, the culture supernatant was discarded and replaced with a 10% CCK-8 solution in each well for 4 h. Subsequently, the absorbance at 450 nm was then recorded using an Enzyme-labeled instrument (CMaxPlus, Molecular Devices, USA).

5-Ethynyl-2′-Deoxyuridine (EdU) Assay

Proliferating cells were detected using the BeyoClick™ EdU Cell Proliferation Kit with AF59 (C0078S, Beyotime), following the manufacturer's protocol. In brief, the treated LLC cells were incubated with 10 µM EdU for 2 h. After that, cells were treated with 4% paraformaldehyde for 10 min, permeabilized in 0.3% Triton X-100 for 20 min, and stained with DAPI solution (C1006, Beyotime) for 5 min. Finally, the fluorescence signals were examined under an inverted fluorescence microscope (Ts2-FC, Nikon), and the percentage of EdU-positive cells was quantified using ImageJ software (version 1.53; NIH, Bethesda, MD, USA).

Cell Apoptosis Analysis

Cell apoptosis of co-cultured LLC cells was assessed using Annexin V-FITC/PI apoptosis analysis kit (556547, BD Pharmingen). Following a wash with pre-cooled PBS, treated LLC cells were resuspended in 500 µL of binding buffer and sequentially stained with 5 µL of Annexin V-FITC for 10 min and 10 µL of PI (C1062L, Beyotime) for 5 min, prior to flow cytometry analysis within 1 h.

Western Blotting

The proteins of cells and tissues were extracted by RIPA Buffer (P0013B, Beyotime, China). The protein concentration was determined using the BCA kit (P0012, Beyotime), followed by separation via 10% SDS-PAGE and transfer to a PVDF membrane. Membrane was treated with 5% milk and incubated with antibody Phospho-STAT1 (AF3299, 1:1000, Affinity), anti-IDO1 and anti-STAT1 (#51851, #9172, 1:1000, Cell Signaling Technology), anti-AHR, anti-Bax, anti-Bcl-2, anti-Cleaved caspase-3, anti-PD-L1 (ab309491, ab32503, ab182858, ab214430, ab213480, 1:1000, Abcam) and anti-GAPDH (10494-1-AP, 1:5000, proteintech) at 4 °C overnight. Post-wash procedures involved incubation with Anti-rabbit IgG, HRP-linked Antibody (7074, 1:6000, CST). Blots were visualized with a chemiluminescent substrate (610020-9Q, Qingxiang, China) and quantified by ImageJ.

Statistical Analysis

Data are expressed as mean ± SD, and analysis using SPSS (v26.0, IBM, IL, USA). All data were presented as statistical comparisons between the two groups, which were performed utilizing an unpaired Student's *t*-test. *ANOVA* was employed to assess differences across multiple groups. Statistical significance was defined as a p-value < 0.05.

Results

Butyrate and PD-1 Inhibitor Co-Combination Suppressed Tumor Growth on LC in Mice

Living fluorescence imaging was utilized to monitor tumor development in mice. Fig. 1A–C illustrates a dramatic decrease in the average and total flux in LC mice following treatment with the PD-1 inhibitor ($p < 0.05$). Remarkably, the inhibitory effect of medium and high doses of NaB with the PD-1 inhibitor on lung cancer was considerably better than that of the PD-1 inhibitor used alone ($p < 0.05$). To explore the synergistic effect of NaB and PD-1 inhibitor on the immune function of LC mice, the thymus index and spleen index were assessed. The model group exhibited lower thymus and spleen indices compared to the control group, while the thymus and spleen indices of the PD-1 group and NaB with PD-1 inhibitor groups showed elevation in contrast to the Model group (Fig. 1D,E, $p < 0.05$). A recent study has shown that butyrate inhibits STAT1 phosphorylation induced by IFN-γ and thereby down-regulates IDO1 expression in nasopharyngeal carcinoma cells [16]. To investigate the synergistic effect of butyrate with a PD-1 inhibitor on lung cancer, we measured IDO1 protein levels using Western blotting. Notably, PD-1 inhibitor treatment decreased the ratio of p-STAT1/STAT1 and the expression of IDO1 and AHR proteins when compared with the model group (Fig. 1F, $p < 0.05$). Interestingly, NaB combined with PD-1 inhibitor dramatically down-regulated the p-STAT1, IDO1, and AHR protein expression when compared with the PD-1 inhibitor alone ($p < 0.05$). These findings indicate that NaB and PD-1 inhibitor synergistically suppressed tumor growth in mice with lung cancer through inhibiting STAT1/IDO1 pathway.

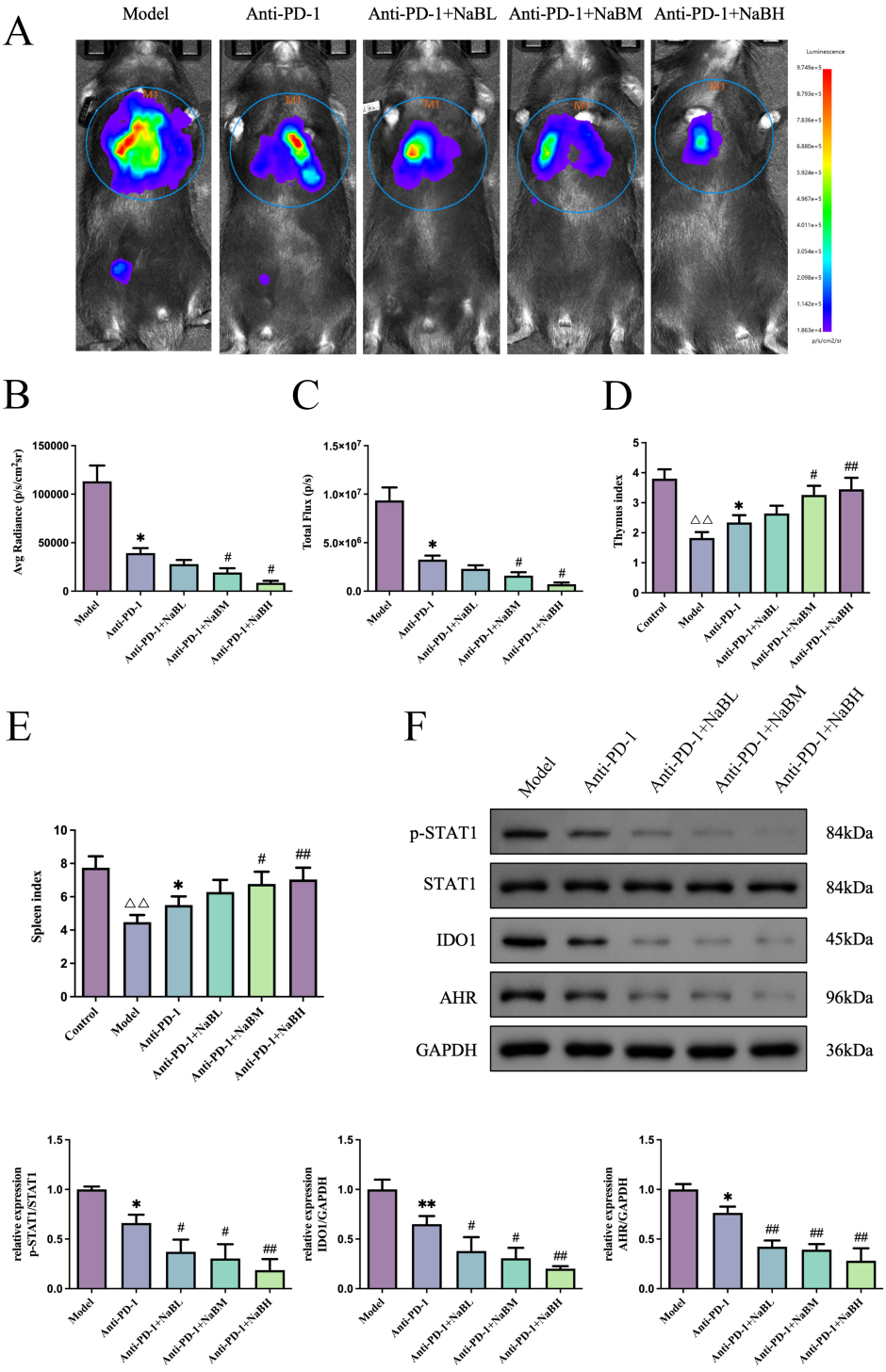

Fig. 1. NaB and PD-1 inhibitor modulate tumor progression in mice through STAT1/IDO1 pathway-driven tryptophan metabolism. (A) Fluorescence imaging of live LC mice. (B,C) The mean and total fluorescence intensity in LC mice. (D,E) The Thymus index and Spleen index in LC mice. (F) The ratio of p-STAT1/STAT1 and the protein expression of IDO1 and AHR in tumor tissues of LC mice. Data were presented as the mean ± SD ($n = 6$). $^{\triangle\triangle}p < 0.01$ compared with the control group; $^{*}p < 0.05$, $^{**}p < 0.01$ compared with the Model group; $^{\#}p < 0.05$, $^{\#\#}p < 0.01$ compared with the Anti-PD-1 group. NaB, sodium butyrate; PD-1, programmed death 1; STAT1, signal transducer and activator of transcription 1; IDO1, Indoleamine 2, 3-dioxygenase 1; LC, Lung cancer; AHR, aryl hydrocarbon receptor; SD, standard deviation.

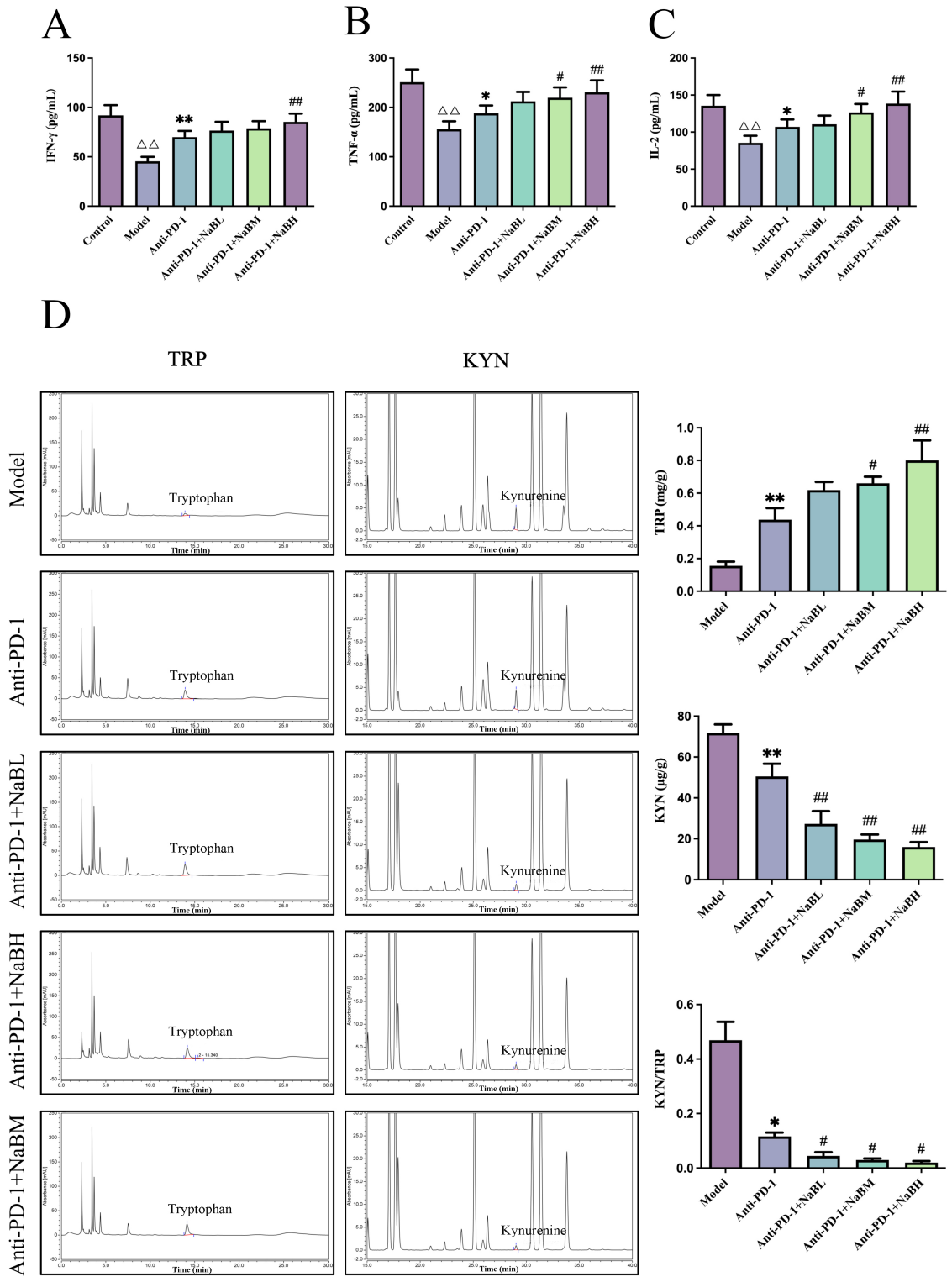

Fig. 2. Effect of NaB combined with PD-1 inhibitor on inflammation and Kyn/Trp ratio in LC mice. (A–C) The serum levels of IFN-γ, TNF-α, and IL-2 levels of mice. (D) Trp and Kyn content in the tumor tissues of LC mice. Data were presented as the mean $\pm$ SD ($n = 6$). $^{\triangle\triangle}p < 0.01$ compared with the control group; $^{*}p < 0.05$, $^{**}p < 0.01$ compared with the Model group; $^{\#}p < 0.05$, $^{\#\#}p < 0.01$ compared with the Anti-PD-1 group. Kyn, kynurenine; Trp, tryptophan; IFN-γ, Interferon-gamma; TNF-α, Tumor necrosis factor alpha; IL-2, Interleukin-2.

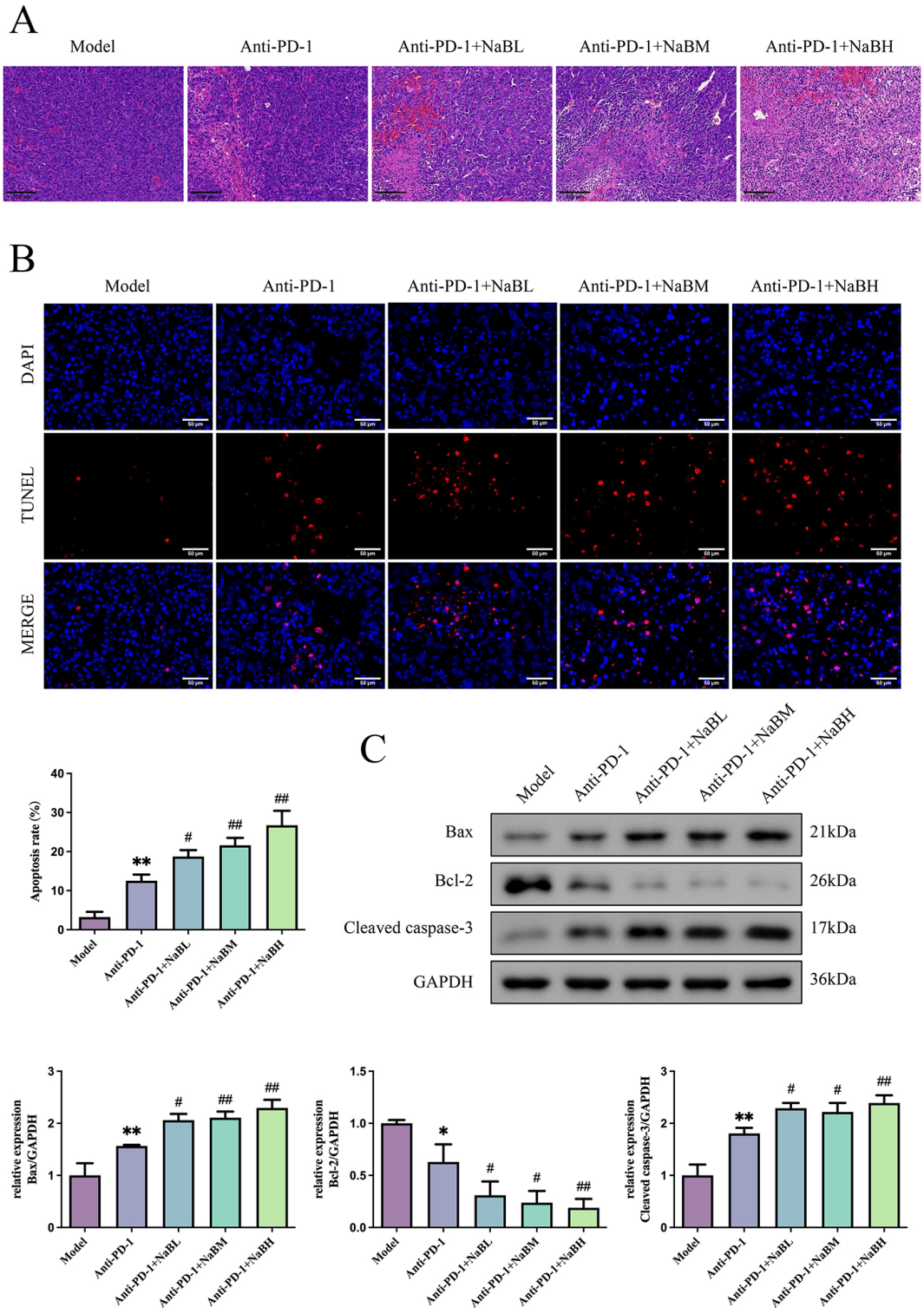

Fig. 3. Effect of NaB combined with PD-1 inhibitors on tumor apoptosis in LC mice. (A) H&E staining of LC mice (scale bar: 100 μm). (B) The apoptosis cells detected by TUNEL. (C) Western Blotting measured Bax, Bcl-2, and Cleaved caspase-3 protein expression in LC mouse tumor tissues. Data were presented as the mean ± SD ($n = 3$). *$p < 0.05$, **$p < 0.01$ compared with the Model group; $^{\#}p < 0.05$, $^{\#\#}p < 0.01$ compared with the Anti-PD-1 group. H&E, hematoxylin and eosin; TUNEL, Terminal deoxynucleotidyl transferase (TdT) dUTP Nick-End Labeling; Bax, Bcl-2-associated X protein; Bcl-2, B-cell lymphoma protein-2.

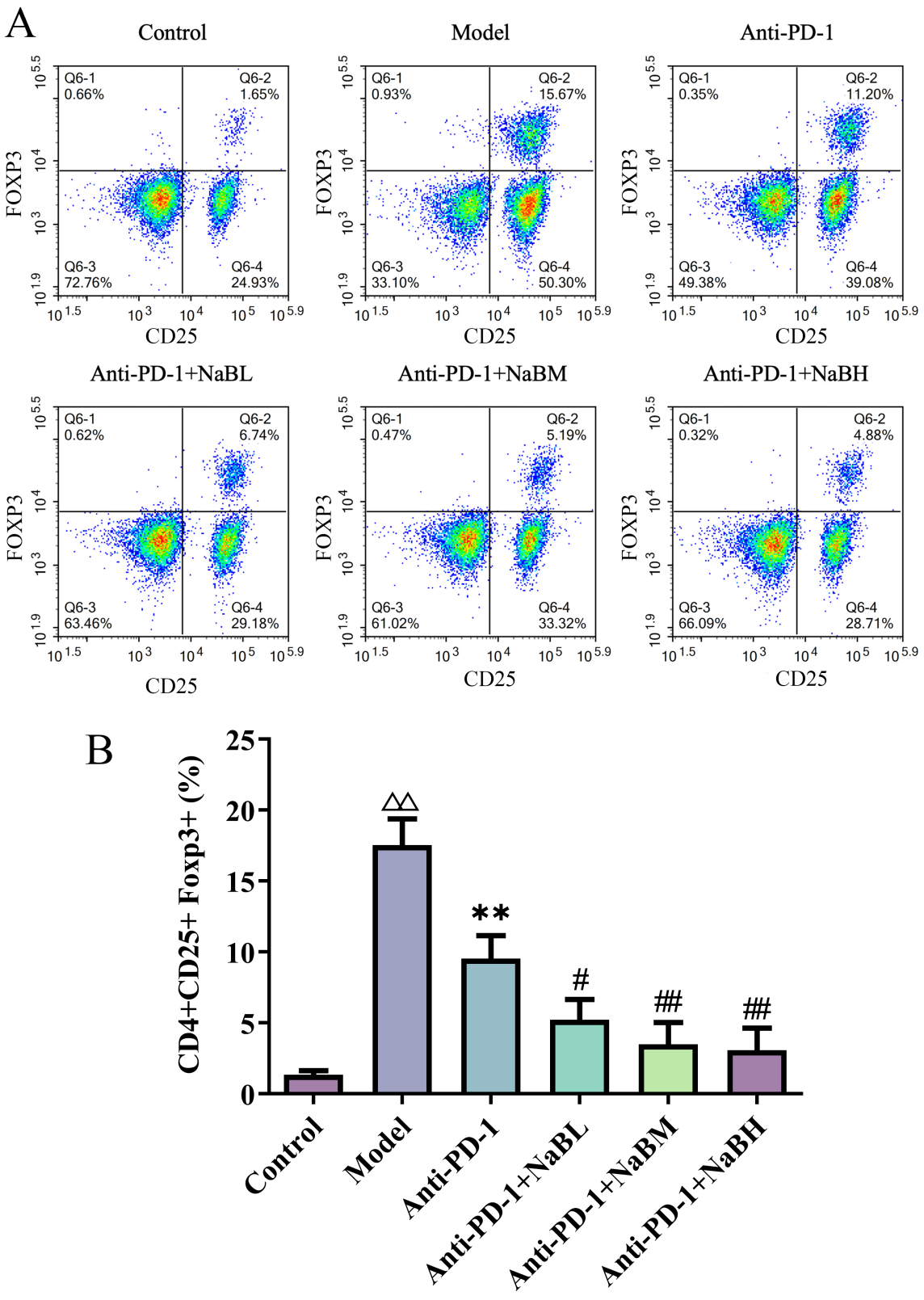

Fig. 4. Effect of NaB and PD-1 inhibitor on Treg proportion change in peripheral blood of LC mice. (A,B) Peripheral blood T cell analysis by flow cytometry in LC mice. Data were presented as the mean ± SD ($n = 6$). $^{\triangle\triangle}p < 0.01$ compared with the control group; $^{**}p < 0.01$ compared with the Model group; $^{\#}p < 0.05$, $^{\#\#}p < 0.01$ compared with the Anti-PD-1 group. Treg, regulatory T.

Butyrate Combined With PD-1 Inhibitor Decreased the Kyn/Trp Level and Elevated Inflammation

IFN-γ is a key regulator of cellular immunity, originating from activated T cells, $\gamma\delta$T cells, and natural killer cells [22]. Targeting proinflammatory cytokines is a key strategy for treating tumors. Therefore, we investigated butyrate and PD-1 inhibitor combination effects on proinflammatory cytokine production in lung cancer cells. Our findings indicated that IFN-γ, TNF-α, and IL-2 serum levels were markedly lower in the Model group than in the Control group. In contrast, treatment with either NaB and PD-1 inhibitor together or PD-1 inhibitor alone markedly elevated serum IFN-γ, TNF-α, and IL-2 levels in LC mice ($p < 0.05$). Besides, the combined application of NaB and PD-1 inhibitor exhibited a significantly superior effect compared to the sole use of the PD-1 inhibitor (Fig. 2A–C, $p < 0.05$).

Furthermore, HPLC detected the Kyn and Trp content in tumor tissues of LC mice. As shown in Fig. 2D, we observed that NaB combined with the PD-1 inhibitor significantly reduced the Kyn/Trp ratios in the Model group ($p < 0.05$). NaB with the PD-1 inhibitor group showed lower Kyn/Trp ratios than PD-1 inhibitor treatment alone ($p < 0.05$). The results demonstrate that NaB with PD-1 blockade modulated immunosuppression through the Try-Kyn pathway.

Butyrate and PD-1 Inhibitor Co-Combination Promoted Tumor Apoptosis in LC Mice

The H&E staining depicted revealed that cancer cells within the Model group were packed closely together, exhibiting the anticipated cellular morphology while demonstrating a scarcity of necrotic cancer cells (Fig. 3A). Conversely, both the anti-PD-1 and anti-PD-1+NaB treatment displayed a marked reduction in tumor cell abundance when compared to the Model group. Besides, TUNEL assay results demonstrated that compared with the Model group, the percentage of apoptotic cells was obviously increased in the anti-PD-1 group. Specifically, different doses of NaB combined with anti-PD-1 inhibitors exerted a synergistic effect to further promote the tumor cell apoptosis rate (Fig. 3B). The administration of PD-1 inhibitor substantially diminished Bcl-2 protein expression while boosting Bax and Cleaved caspase-3 protein concentrations in mice with lung cancer. Notably, the combination treatment involving anti-PD-1 and sodium butyrate proved to be a far more potent catalyst for tumor cell apoptosis than the PD-1 inhibitor regimen alone (Fig. 3C, $p < 0.05$). Altogether, these results suggest that NaB, when used in conjunction with PD-1 inhibitors, promoted tumor apoptosis in LC mice.

Butyrate Decreased the Proportion of Treg Cells and Enhanced T-Cell Infiltration in LC Mice Treated With PD-1 Inhibitor Through the Suppression of STAT1/IDO1 Pathway

Flow cytometry was used to assess the impact of NaB and PD-1 inhibitor co-treatment on the Treg cells in the peripheral blood of LC mice. Fig. 4A,B illustrates a significant increase in population of Treg cells between the Model group and the Control group ($p < 0.05$). Surprisingly, NaB combined with the PD-1 inhibitor more effectively reversed regulatory T cell populations in LC mice compared to PD-1 inhibitor alone ($p < 0.05$). Further IHC staining assessed the impact of combining butyrate with PD-1 inhibitor on T-cell tumor infiltration. In the Model group, a marked rise in $CD8^+$ and $CD4^+$ T cell counts post-PD-1 inhibitor therapy was noted, as anticipated. Furthermore, anti-PD-1 therapy combined with varying NaB doses markedly enhanced $CD8^+$ and $CD4^+$ T-cell populations relative to the PD-1 inhibitor alone (Fig. 5A–C, $p < 0.05$). Interestingly, different dosages of NaB combined with PD-1 inhibitor-treated tumors attenuated the phosphorylation of STAT1 and reduced IDO1 expression in mice when compared with the PD-1 inhibitor alone (Fig. 5A,D,E, $p < 0.05$). Taken together, our findings underscore that butyrate, when used alongside the PD-1 inhibitor, boosted T cell infiltration into tumor tissues, at least in part, which was associated with the suppression of the STAT1/IDO1 signaling pathway.

2-NP or FICZ Diminished the Suppressive Effect of NaB Combined With PD-1 Inhibitor on LC In Vitro

To examine STAT1 and AhR involvement in NaB-PD-1 inhibitor synergy against lung cancer, we conducted rescue assays using $CD8^+$ T cells co-cultured with lung cancer cells. Initially, prior to immunomagnetic bead separation, the proportion of the $CD8^+$ T lymphocyte subset ($CD3^+/CD8^+$) in mouse splenic tissue was $11.73\% \pm 0.78\%$. After isolation, the proportion of $CD8^+$ T lymphocytes ($CD3^+/CD8^+$) increased to $97.51\% \pm 1.51\%$, demonstrating a high purity of the extracted $CD8^+$ T cells (Fig. 6A). As expected, the $CD8^+$ group showed a moderate reduction in cell viability compared to the Control group. However, combining $CD8^+$ T cells with PD-1 blockade further decreased the viability of LLC cell. Specifically, NaB combined with PD-1 blockade potentiated $CD8^+$ T-cell suppression of LLC cell proliferation (Fig. 6B, $p < 0.05$). However, 2-NP or FICZ abolished the growth inhibitory effect of $CD8^+$ T cells on LLC cells promoted by NaB combined with PD-1 treatment. Consistently, NaB combined with PD-1 inhibition markedly reduced EdU-positive proliferative $CD8^+$ T cells, whereas 2-NP or FICZ treatment notably enhanced this proliferation in co-cultures with LC cells (Fig. 6C, $p < 0.05$). Taken together, these data suggest that NaB coupled with PD-1 inhibitors potentiates $CD8^+$ T cells-mediated suppression of Lung cancer cell viability and proliferation by suppressing the STAT1/AhR pathway.

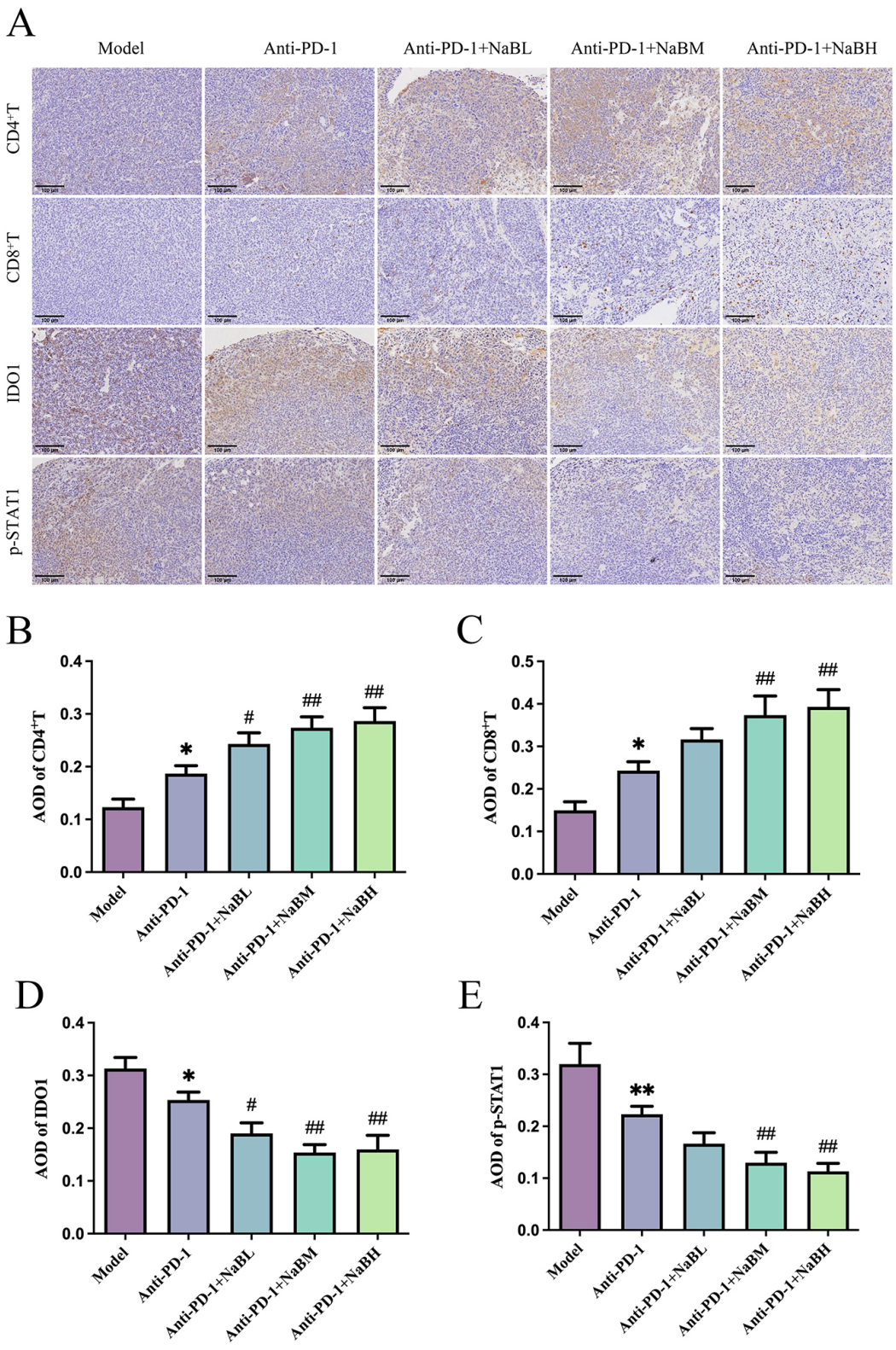

Fig. 5. Effect of NaB combined with PD-1 inhibitor on infiltration of T-cells in LC mice. (A) IHC staining of $CD4^+$T, $CD8^+$T, IDO1, and p-STAT1 in lung tumor sections (Scale bar, 100 μm). (B–E) Average optical density (AOD) of $CD4^+$T, $CD8^+$T, IDO1, and p-STAT1 as a percentage of marker-positive area in IHC-stained lung tumors. Data were presented as the mean ± SD ($n = 3$). *$p < 0.05$, **$p < 0.01$ compared with the Model group; $^{\#}p < 0.05$, $^{\#\#}p < 0.01$ compared with the Anti-PD-1 group. IHC, Immunohistochemistry.

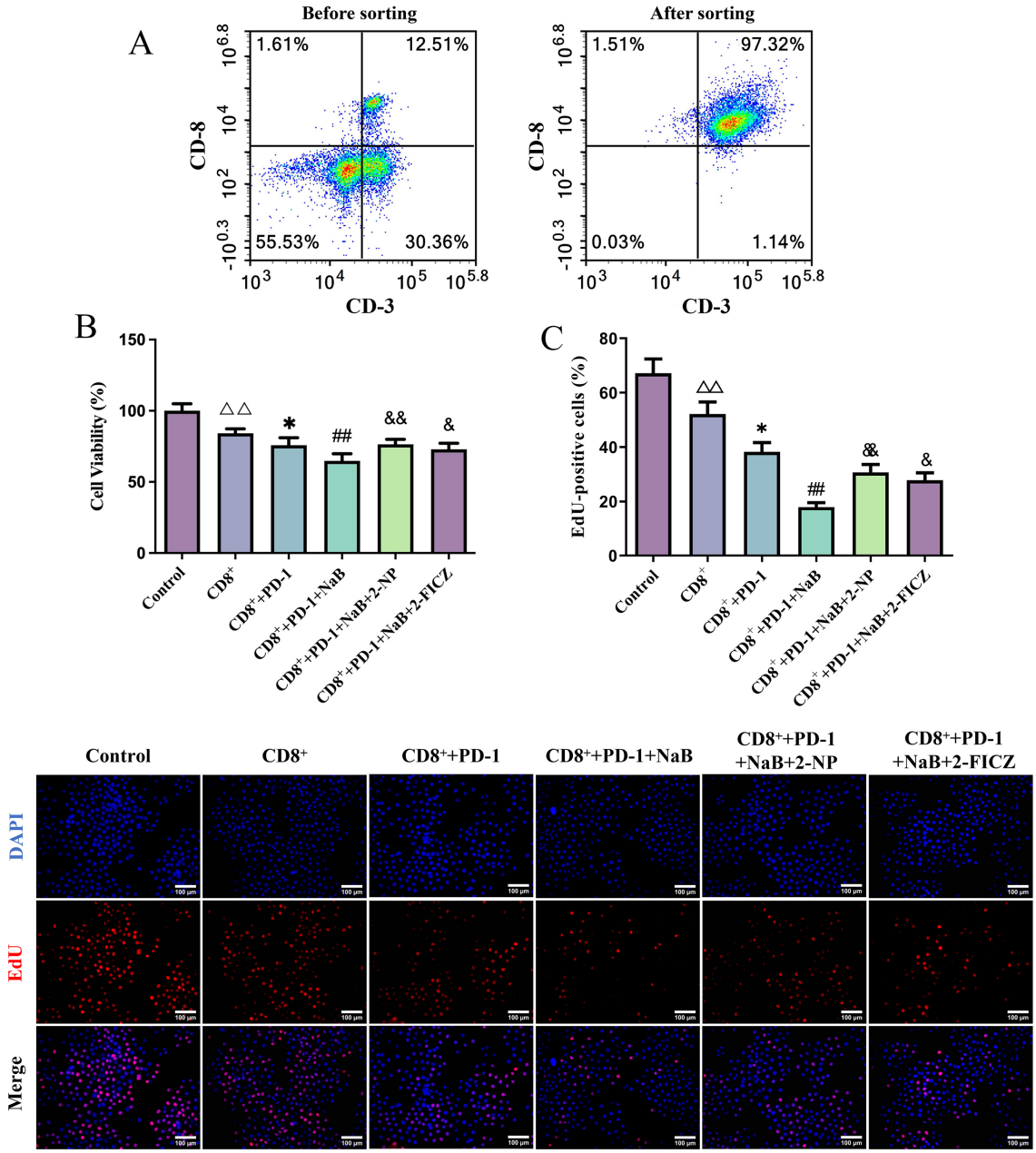

Fig. 6. Effect of 2-NP or FICZ on the anticancer activity of NaB and PD-1 inhibitor efficacy against CD8$^+$ T cell co-cultured with LC cells. (A) Proportions of CD3$^+$/CD8$^+$ T lymphocyte cell subsets before and after separated immue with magnetic bead method detected by flow cytometry. (B) The cell viability of CD8$^+$ T cells co-cultured with LC cells. (C) The cell proliferation analysis in CD8$^+$ T cells co-cultured with LC cells using EdU staining. Data were presented as the mean ± SD (n = 3). $^{\triangle\triangle}p < 0.01$ compared with the control group; $^{*}p < 0.05$, compared with the CD8$^+$ group; $^{\#\#}p < 0.01$ compared with the CD8$^+$+PD-1 group. $^{\&}p < 0.05$, $^{\&\&}p < 0.01$ compared with the CD8$^+$+PD-1+NaB group. 2-NP, 2-(1, 8-Naphthyridin-2-yl)phenol; FICZ, 6-Formylindolo[3, 2-b]carbazole; EdU, 5-Ethynyl-2′-Deoxyuridine.

2-NP or FICZ Reversed the Effect of NaB Coupled With PD-1 Inhibitor in Apoptosis and Trp-Kyn Metabolism in CD8$^+$ T Cells Co-Cultured With LLC Cells

As shown in Fig. 7A, the combination of NaB and a PD-1 inhibitor promoted the pro-apoptotic effect of CD8$^+$ T cells on LC cells, while 2-NP or FICZ treatment abolished the pro-apoptotic effect of CD8$^+$ T cells with NaB coupled with PD-1 inhibitor ($p < 0.05$). Meanwhile, Kyn levels significantly decreased in CD8$^+$ T cells, with the PD-1 inhibitor and CD8$^+$ T cells combination further reducing Kyn levels. NaB and PD-1 inhibitor co-treatment showed a combined effect to enhance the effect of CD8$^+$ T cells in decreasing the Kyn levels in LC cells. Moreover, 2-NP

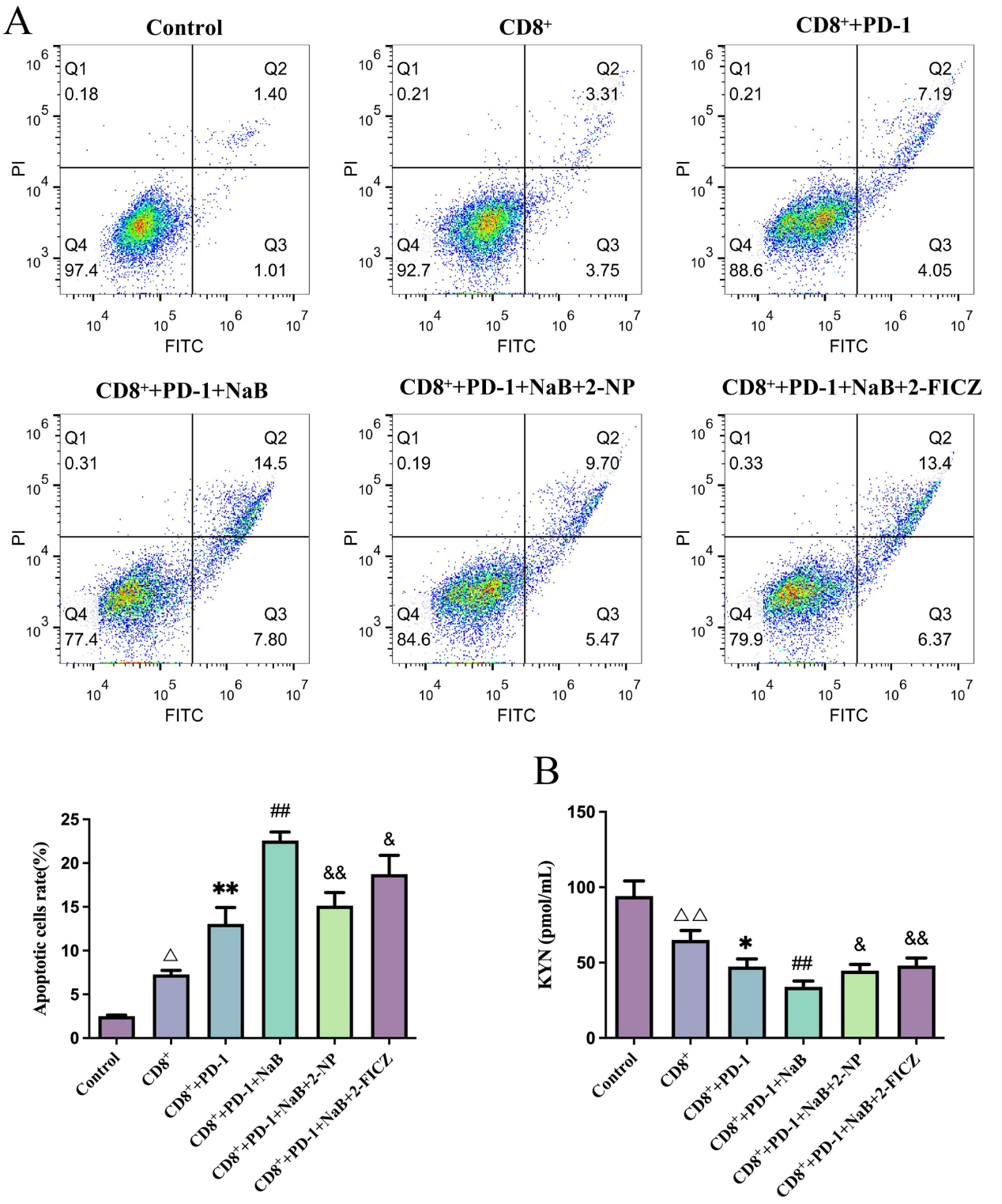

Fig. 7. Effect of 2-NP or FICZ on the anti-apoptosis effect and content of Kyn levels of NaB combined with PD-1 inhibitor in CD8$^+$ T cells co-cultured with LLC cells. (A) Flow cytometric analysis of cell apoptosis in LC cells with different treatments. (B) The Kyn content of cell culture supernatant in LLC cells co-cultured with CD8$^+$ T cells was measured by ELISA assays. Data were presented as the mean ± SD ($n = 3$). $^{\triangle}p < 0.05$, $^{\triangle\triangle}p < 0.01$ compared with the control group; $^{*}p < 0.05$, $^{**}p < 0.01$ compared with the CD8$^+$ group; $^{\#\#}p < 0.01$ compared with the CD8$^+$+PD-1 group. $^{\&}p < 0.05$, $^{\&\&}p < 0.01$ compared with the CD8$^+$+PD-1+NaB group. LLC, Lewis lung carcinoma; ELISA, Enzyme-linked immunosorbent assay.

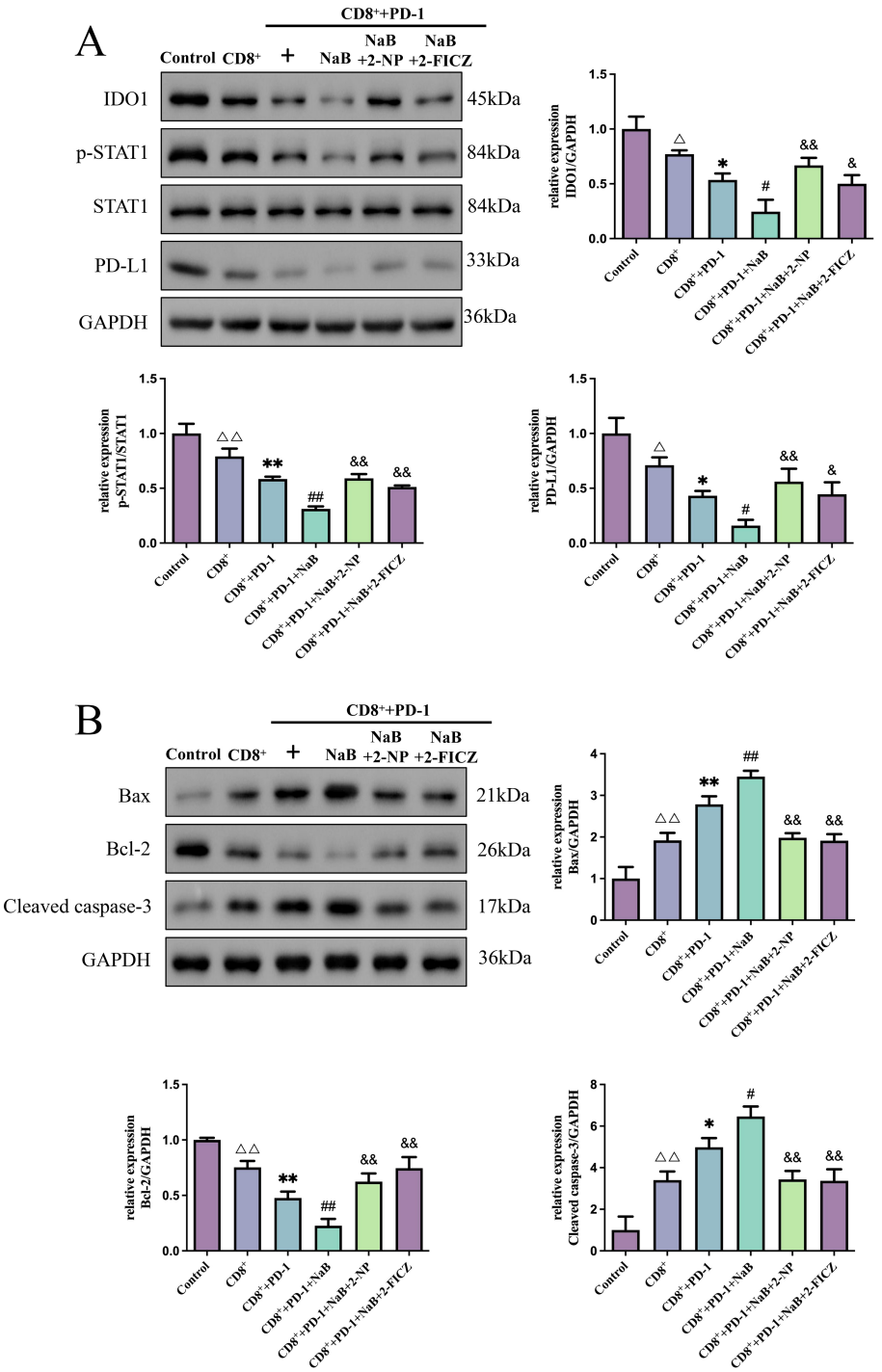

Fig. 8. Effect of 2-NP or FICZ on the STAT1/IDO1-Trp-Kyn pathway inhibition in CD8$^+$ T cells co-cultured with LC cells under NaB combined with a PD-1 inhibitor. (A) The ratio of p-STAT1/STAT1 and the protein expression of IDO1 and AHR in LLC cells. (B) The protein expression of Bax, Bcl-2, and Cleaved caspase-3 in LLC cells. Data were presented as the mean ± SD (n = 3). $^{\triangle}p < 0.05$, $^{\triangle\triangle}p < 0.01$ compared with the control group; $^{*}p < 0.05$, $^{**}p < 0.01$ compared with the CD8$^+$ group; $^{\#}p < 0.05$, $^{\#\#}p < 0.01$ compared with the CD8$^+$+PD-1 group. $^{\&}p < 0.05$, $^{\&\&}p < 0.01$ compared with the CD8$^+$+PD-1+NaB group. 2-NP, 2-(1, 8-Naphthyridin-2-yl)phenol; FICZ, 6-Formylindolo[3, 2-b]carbazole; NaB, sodium butyrate; PD-1, programmed death 1; STAT1, signal transducer and activator of transcription 1; IDO1, Indoleamine 2, 3-dioxygenase 1; LC, Lung cancer; LLC, Lewis lung carcinoma; AHR, aryl hydrocarbon receptor; Bax, Bcl-2-associated X protein; Bcl-2, B-cell lymphoma protein-2.

or FICZ significantly abolished the promoted effect of NaB and PD-1 inhibitor co-administration on the decreased Kyn levels of $CD8^+$ T cells (Fig. 7B, $p < 0.05$).

Western blot results showed a marked decrease in IDO1 and PD-L1 protein expression, as well as the ratio of p-STAT1/STAT1 in the $CT8^+$ +PD-1 inhibitor group compared to the $CT8^+$ group. NaB with PD-1 blockade enhanced suppression of IDO1, p-STAT1, and PD-L1 protein levels in LLC cells relative to $CT8^+$ T cells (Fig. 8A, $p < 0.05$). However, 2-NP or FICZ treatment increased the protein expression of IDO1, p-STAT1, and PD-L1 in the $CD8^+$ +PD-1 and NaB group. Furthermore, the protein levels of Bax and Cleaved caspase-3 showed a marked increase, whereas Bcl-2 expression demonstrated a significant decrease in $CD8^+$ T cells that had been cultured alongside LLC cells when compared to the Control group (Fig. 8B, $p < 0.05$). Notably, the synergistic effect of NaB and PD-1 inhibitor upregulated Bax and Cleaved caspase-3 protein expression in $CT8^+$ T cells against tumor cells. However, 2-NP or FICZ treatment counteracted this synergistic effect of NaB and PD-1 inhibitor. Collectively, our data demonstrate that combining NaB with PD-1 inhibitor works in concert to trigger apoptosis in lung cancer cells, suppress the Try-Kyn metabolic axis, and ramp up the cancer-fighting prowess of $CD8^+$ T cells by putting the brakes on the STAT1/IDO1-driven Try-Kyn signaling pathway.

Discussion

PD-1 inhibitors, which target PD-1/PD-L1 interaction, have the potential to shrink tumors in a select group of NCLC patients. However, the success rate in clinical trials hovers around a mere 25% [23]. Consequently, the urgency of investigating innovative therapeutic strategies to amplify the effectiveness of immunotherapy in medical use is pronounced. Clinical studies have found that the relative abundance of *Akkermansia muciniphila* in cancer patients is significantly correlated with the response to ICI, and oral administration of *Akkermansia muciniphila* can restore the response of patients to PD-1 inhibitor [24]. It is shown to enhance the synthesis of short-chain fatty acids, including butyric, propionic, and acetic acids, in the gut. Short-chain fatty acids, while crucial for upholding cellular balance, also play a pivotal part in the development and advancement of cancer [25].

Prior research showed that in human cancer patients, patients responding to oxaliplatin had elevated serum butyrate levels compared to non-responders [12]. Additionally, this may enhance the manifestation and activity of ID2 in human $CD8^+$ T cells irrespective of anti-PD-1 treatment. In accordance with previous findings, we found NaB can promote anti-PD-1 immunotherapy efficacy by inhibiting tumor growth, elevating pro-inflammatory factors levels, and reducing the Kyn/Trp ratio *in vivo*. Butyrate combined with the PD-1 inhibitor also promotes tumor apoptosis in LC mice. In contrast to the control group, the combination treatment involving Butyrate and the PD-1 inhibitor showed a marked boost in both $CD8^+$ and $CD4^+$ T cell populations. These findings strongly indicate that Butyrate's anti-tumor activity primarily works its magic by engaging with the PD-1 pathway in $CD8^+$ T cells while also interacting with the Trp-Kyn metabolic route.

The essential amino acid tryptophan has emerged as a crucial regulator of cancer progression because of its regulatory function in immune cell activity. Trp catabolism has turned into an essential metabolic regulator of cancer progression [26]. IDO1 catalyzes the degradation of Trp into Kyn, thereby regulating immune responses and promoting cancer progression. Mechanistically, the IDO1 inhibitor is anticipated to modulate the microenvironment and potentiate the action of immune effectors [27]. However, IDO1 inhibition alone has a negligible anticancer effect in most cancer patients. Notably, adding IDO1 inhibitors to PD-1 or PD-L1 enhances the efficacy of checkpoint blockade alone, showing encouraging response rates and response durability [28]. Consequently, IDO1 inhibitors enable the jump-starting of T and NK cell activity while effectively dismantling the tumor's immune evasion tactics. Within the IFN-γ receptor's cytoplasmic tail, JAK kinase kick-starts the STAT1 pathway, which then zeroes in on the GAS sequence to directly spur IDO1 transcription [29]. Here, we used the 2-NP and FICZ to further elaborate on the mechanism of NaB and PD-1 inhibitor co-administration in lung tumor tissues. Combination therapy decreased STAT1 phosphorylation and IDO1 protein expression in lung tumors and LLC cells, contrasting with the effects of PD-1 monotherapy. Furthermore, our research demonstrated that NaB plus the PD-1 inhibitors decreased cell viability and Kyn levels while accelerating apoptosis in LLC cells. Our findings indicate NaB enhances PD-1's anti-tumor activity in lung cancer through the IDO1/STAT1 pathway.

Enormous studies revealed that $CD8^+$ T cells within tumor tissues undergo activation in response to antigenic stimulation, and the availability of IL-2 in the tumor microenvironment not only helps them transform into killer T cells but also ramps up their ability to infiltrate the tumor site [30,31]. PD-1 blockade elevates the frequency of the $CD8^+$ effector memory T-cell subset and rejuvenates T-cell expansion as well as effector function, thereby resulting in tumor eradication [32,33]. Among the effectors of rejuvenated exhausted T cells, increased IFN-γ expression is a common feature in tumors responding to immune checkpoint blockade. IFN-γ suppresses cancer cell growth and triggers apoptosis in certain malignancies while also promoting tumor immune evasion, resulting in resistance to anti-PD-1 immunotherapy [34,35]. The immune escape induced by IFN-γ is mediated by multiple mechanisms, such as down-regulating tumor antigen expression and up-regulating PD-L1 and IDO1 expression in tumor cells [36]. Our findings revealed that the combination of

NaB and PD-1 inhibitor enhances the functional phenotype of $CD8^+$ T-cells and elevates the levels of IFN-γ, IL-2, and TNF-α in LC mice. These findings suggest that NaB, in conjunction with PD-1 inhibitors, facilitates the infiltration of $CD8^+$ T cells and the release of IFN-γ, thus suppressing the tumor. Nevertheless, the combined antitumor activity of NaB and PD-1 was negated upon administration of 2-NP or FICZ. The study demonstrated the enhancement of PD-1 inhibitors' anti-tumor activity in lung cancer through NaB therapy, which modulates the STAT1/IDO1 pathway. Despite the insights provided by our findings, a number of questions remain unanswered. The exact mechanisms by which the combination of butyrate and PD-1 inhibitors causes inhibition of the tryptophan-kynurenine pathway remain to be fully elucidated. Moreover, the lack of an agonist-alone control group *in vitro* is a limitation of this work. Additionally, while *in vivo* bioimaging provided valuable longitudinal data, future studies will include *ex vivo* fluorescence imaging of excised lungs to obtain a more quantitative and high-resolution analysis of metastatic burden. Finally, exploring combinations with other short-chain fatty acids warrants examination.

Conclusion

In summary, our results indicate that the combination of butyrate and PD-1 inhibitors enhances $CD8^+$ T cell tumor infiltration by disrupting the STAT1/IDO1 tryptophan-kynurenine pathway, thereby mitigating immunosuppression in lung cancer. Our study provides preclinical evidence for a novel combination therapy comprising ICIs and NaB for anti-lung cancer treatment.

Availability of Data and Materials

The datasets used and/or analysed during the current study are available from the corresponding author on reasonable request.

Author Contributions

CCL: Conceptualization, Funding acquisition, Formal analysis, Investigation, Writing—original draft; XXL: Investigation, Data curation, Writing-review & editing; BM: Investigation, Formal analysis, Writing-review & editing; FY: Investigation, Formal analysis, Writing-review & editing; SZW: Investigation, Formal analysis, Writing-review & editing; WXL: Conceptualization, Project administration, Writing—review & editing. All authors give final approval of the version to be published. All authors have participated sufficiently in the work to take public responsibility for appropriate portions of the content and agreed to be accountable for all aspects of the work in ensuring that questions related to its accuracy or integrity.

Ethics Approval and Consent to Participate

This study protocol was reviewed and approved by Laboratory animal management and ethics committee of Hangzhou Hunter Testing Biotechnology Co., Ltd. (Approval number: IACUC/HTYJ-8201-80). The design of the study, the methods used in the experiments, and the presentation of findings adhere to the ARRIVE guidelines to guarantee the integrity and reproducibility of animal research.

Acknowledgment

Not applicable.

Funding

This work was supported by grants from the Zhejiang Provincial Medical and Health Science Research Fund (2024KY607).

Conflict of Interest

The authors declare no conflict of interest.

References

[1] Smolarz B, Łukasiewicz H, Samulak D, Piekarska E, Kołaciński R, Romanowicz H. Lung Cancer-Epidemiology, Pathogenesis, Treatment and Molecular Aspect (Review of Literature). International Journal of Molecular Sciences. 2025; 26: 2049. https://doi.org/10.3390/ijms26052049.

[2] Stravopodis DJ, Papavassiliou KA, Papavassiliou AG. Vistas in Non-Small Cell Lung Cancer (NSCLC) Treatment: of Kinome and Signaling Networks. International Journal of Biological Sciences. 2023; 19: 2002–2005. https://doi.org/10.7150/ijbs.83574.

[3] Shiraishi Y, Nomura S, Sugawara S, Horinouchi H, Yoneshima Y, Hayashi H, *et al*. Comparison of platinum combination chemotherapy plus pembrolizumab versus platinum combination chemotherapy plus nivolumab-ipilimumab for treatment-naive advanced non-small-cell lung cancer in Japan (JCOG2007): an open-label, multicentre, randomised, phase 3 trial. The Lancet. Respiratory Medicine. 2024; 12: 877–887. https://doi.org/10.1016/S2213-2600(24)00185-1.

[4] Arbour KC, Riely GJ. Systemic Therapy for Locally Advanced and Metastatic Non-Small Cell Lung Cancer: A Review. JAMA. 2019; 322: 764–774. https://doi.org/10.1001/jama.2019.11058.

[5] Orosz Z, Kovács Á. The role of chemoradiotherapy and immunotherapy in stage III NSCLC. Pathology and Oncology Research. 2024; 30: 1611716. https://doi.org/10.3389/pore.2024.1611716.

[6] Huang Z, Wang J, Xia Z, Lv Q, Ruan Z, Dai Y. Wnt/β-Catenin Pathway-Mediated *PD-L1* Overexpression Facilitates the Resistance of Non-Small Cell Lung Cancer Cells to Epidermal Growth Factor Receptor Tyrosine Kinase Inhibitors. Discovery Medicine. 2024; 36: 2300–2308. https://doi.org/10.24976/Discov.Med.202436190.211.

[7] Dammeijer F, van Gulijk M, Mulder EE, Lukkes M, Klaase L, van den Bosch T, *et al*. The PD-1/PD-L1-Checkpoint Restrains T cell Immunity in Tumor-Draining Lymph Nodes. Cancer Cell.

2020; 38: 685–700.e8. https://doi.org/10.1016/j.ccell.2020.09.001.

[8] Zhang JY, Yan YY, Li JJ, Adhikari R, Fu LW. PD-1/PD-L1 Based Combinational Cancer Therapy: Icing on the Cake. Frontiers in Pharmacology. 2020; 11: 722. https://doi.org/10.3389/fphar.2020.00722.

[9] Mir R, Albarqi S, Albalawi W, Alanazi G, Alsubaie S, Alghaban R, *et al*. Emerging Role of Gut Microbiome and Risk of Developing Colorectal Cancer and Its Implications in Treatment. Discovery Medicine. 2025; 37: 1176–1199. https://doi.org/10.24976/Discov.Med.202537198.105.

[10] Dizman N, Meza L, Bergerot P, Alcantara M, Dorff T, Lyou Y, *et al*. Nivolumab plus ipilimumab with or without live bacterial supplementation in metastatic renal cell carcinoma: a randomized phase 1 trial. Nature Medicine. 2022; 28: 704–712. https://doi.org/10.1038/s41591-022-01694-6.

[11] Hui W, Yu D, Cao Z, Zhao X. Butyrate inhibit collagen-induced arthritis via Treg/IL-10/Th17 axis. International Immunopharmacology. 2019; 68: 226–233. https://doi.org/10.1016/j.intimp.2019.01.018.

[12] He Y, Fu L, Li Y, Wang W, Gong M, Zhang J, *et al*. Gut microbial metabolites facilitate anticancer therapy efficacy by modulating cytotoxic $CD8^+$ T cell immunity. Cell Metabolism. 2021; 33: 988–1000.e7. https://doi.org/10.1016/j.cmet.2021.03.002.

[13] Kaźmierczak-Siedlecka K, Marano L, Merola E, Roviello F, Połom K. Sodium butyrate in both prevention and supportive treatment of colorectal cancer. Frontiers in Cellular and Infection Microbiology. 2022; 12: 1023806. https://doi.org/10.3389/fcimb.2022.1023806.

[14] Karim MR, Iqbal S, Mohammad S, Morshed MN, Haque MA, Mathiyalagan R, *et al*. Butyrate's (a short-chain fatty acid) microbial synthesis, absorption, and preventive roles against colorectal and lung cancer. Archives of Microbiology. 2024; 206: 137. https://doi.org/10.1007/s00203-024-03834-7.

[15] Zhu X, Li K, Liu G, Wu R, Zhang Y, Wang S, *et al*. Microbial metabolite butyrate promotes anti-PD-1 antitumor efficacy by modulating T cell receptor signaling of cytotoxic CD8 T cell. Gut Microbes. 2023; 15: 2249143. https://doi.org/10.1080/19490976.2023.2249143.

[16] Martin-Gallausiaux C, Larraufie P, Jarry A, Béguet-Crespel F, Marinelli L, Ledue F, *et al*. Butyrate Produced by Commensal Bacteria Down-Regulates *Indolamine 2,3-Dioxygenase 1* (*IDO-1*) Expression *via* a Dual Mechanism in Human Intestinal Epithelial Cells. Frontiers in Immunology. 2018; 9: 2838. https://doi.org/10.3389/fimmu.2018.02838.

[17] Platten M, Nollen EAA, Röhrig UF, Fallarino F, Opitz CA. Tryptophan metabolism as a common therapeutic target in cancer, neurodegeneration and beyond. Nature Reviews. Drug Discovery. 2019; 18: 379–401. https://doi.org/10.1038/s41573-019-0016-5.

[18] Shi D, Wu X, Jian Y, Wang J, Huang C, Mo S, *et al*. USP14 promotes tryptophan metabolism and immune suppression by stabilizing IDO1 in colorectal cancer. Nature Communications. 2022; 13: 5644. https://doi.org/10.1038/s41467-022-33285-x.

[19] Campesato LF, Budhu S, Tchaicha J, Weng CH, Gigoux M, Cohen IJ, *et al*. Blockade of the AHR restricts a Treg-macrophage suppressive axis induced by L-Kynurenine. Nature Communications. 2020; 11: 4011. https://doi.org/10.1038/s41467-020-17750-z.

[20] Chen Z, Ding YH, Shao L, Ji XM, Qian X, Zhang AQ. Qingfei mixture mitigates immunosuppression of tumor microenvironment in non-small cell lung cancer by blocking stat1/Ido1-mediated tryptophan-kynurenine pathway. Heliyon. 2024; 10: e32260. https://doi.org/10.1016/j.heliyon.2024.e32260.

[21] Yin X, Sun X, Li A, Ruan J, Niu H, Zhou Y, *et al*. Wenxia Changfu formula inhibits Lewis lung cancer metastasis by reprogramming tumor-associated macrophages through the PPAR-γ/CD36 pathway. Journal of Ethnopharmacology. 2025; 351: 120103. https://doi.org/10.1016/j.jep.2025.120103.

[22] Fang C, Weng T, Hu S, Yuan Z, Xiong H, Huang B, *et al*. IFN-γ-induced ER stress impairs autophagy and triggers apoptosis in lung cancer cells. Oncoimmunology. 2021; 10: 1962591. https://doi.org/10.1080/2162402X.2021.1962591.

[23] Li HY, McSharry M, Bullock B, Nguyen TT, Kwak J, Poczobutt JM, *et al*. The Tumor Microenvironment Regulates Sensitivity of Murine Lung Tumors to PD-1/PD-L1 Antibody Blockade. Cancer Immunology Research. 2017; 5: 767–777. https://doi.org/10.1158/2326-6066.CIR-16-0365.

[24] Routy B, Le Chatelier E, Derosa L, Duong CPM, Alou MT, Daillère R, *et al*. Gut microbiome influences efficacy of PD-1-based immunotherapy against epithelial tumors. Science (New York, N.Y.). 2018; 359: 91–97. https://doi.org/10.1126/science.aan3706.

[25] Chen HH, Wu QJ, Zhang TN, Zhao YH. Gut microbiome and serum short-chain fatty acids are associated with responses to chemo- or targeted therapies in Chinese patients with lung cancer. Frontiers in Microbiology. 2023; 14: 1165360. https://doi.org/10.3389/fmicb.2023.1165360.

[26] Kober C, Roewe J, Schmees N, Roese L, Roehn U, Bader B, *et al*. Targeting the aryl hydrocarbon receptor (AhR) with BAY 2416964: a selective small molecule inhibitor for cancer immunotherapy. Journal for Immunotherapy of Cancer. 2023; 11: e007495. https://doi.org/10.1136/jitc-2023-007495.

[27] Jung KH, LoRusso P, Burris H, Gordon M, Bang YJ, Hellmann MD, *et al*. Phase I Study of the Indoleamine 2,3-Dioxygenase 1 (IDO1) Inhibitor Navoximod (GDC-0919) Administered with PD-L1 Inhibitor (Atezolizumab) in Advanced Solid Tumors. Clinical Cancer Research: an Official Journal of the American Association for Cancer Research. 2019; 25: 3220–3228. https://doi.org/10.1158/1078-0432.CCR-18-2740.

[28] Charehjoo A, Majidpoor J, Mortezaee K. Indoleamine 2,3-dioxygenase 1 in circumventing checkpoint inhibitor responses: Updated. International Immunopharmacology. 2023; 118: 110032. https://doi.org/10.1016/j.intimp.2023.110032.

[29] Shu G, Chen M, Liao W, Fu L, Lin M, Gui C, *et al*. PABPC1L Induces IDO1 to Promote Tryptophan Metabolism and Immune Suppression in Renal Cell Carcinoma. Cancer Research. 2024; 84: 1659–1679. https://doi.org/10.1158/0008-5472.CAN-23-2521.

[30] Spolski R, Li P, Leonard WJ. Biology and regulation of IL-2: from molecular mechanisms to human therapy. Nature Reviews. Immunology. 2018; 18: 648–659. https://doi.org/10.1038/s41577-018-0046-y.

[31] Hashimoto M, Araki K, Cardenas MA, Li P, Jadhav RR, Kissick HT, *et al*. PD-1 combination therapy with IL-2 modifies $CD8^+$ T cell exhaustion program. Nature. 2022; 610: 173–181. https://doi.org/10.1038/s41586-022-05257-0.

[32] Ahn E, Araki K, Hashimoto M, Li W, Riley JL, Cheung J, *et al*. Role of PD-1 during effector CD8 T cell differentiation. Proceedings of the National Academy of Sciences of the United States of America. 2018; 115: 4749–4754. https://doi.org/10.1073/pnas.1718217115.

[33] Ribas A, Shin DS, Zaretsky J, Frederiksen J, Cornish A, Avramis E, *et al*. PD-1 Blockade Expands Intratumoral Memory T Cells. Cancer Immunology Research. 2016; 4: 194–203. https://doi.org/10.1158/2326-6066.CIR-15-0210.

[34] Ye F, Cai Z, Wang B, Zeng C, Xi Y, Hu S, *et al*. TGFβ Antagonizes IFNγ-Mediated Adaptive Immune Evasion via Activation of the AKT-Smad3-SHP1 Axis in Lung Adenocarcinoma. Cancer Research. 2023; 83: 2262–2277. https://doi.org/10.1158/0008-5472.CAN-22-3009.

[35] Liu K, Huang J, Liu J, Li C, Kroemer G, Tang D, *et al*. HSP90

Mediates IFNγ-Induced Adaptive Resistance to Anti-PD-1 Immunotherapy. Cancer Research. 2022; 82: 2003–2018. https://doi.org/10.1158/0008-5472.CAN-21-3917.

[36] Zhang ML, Kem M, Mooradian MJ, Eliane JP, Huynh TG, Iafrate AJ, *et al*. Differential expression of PD-L1 and IDO1 in association with the immune microenvironment in resected lung adenocarcinomas. Modern Pathology: an Official Journal of the United States and Canadian Academy of Pathology, Inc. 2019; 32: 511–523. https://doi.org/10.1038/s41379-018-0160-1.